Zn, Mn and Te K-edge EXAFS studies of the diluted magnetic semiconductor $Zn_{1-x}Mn_xTe$

1996 J. Phys.: Condens. Matter 8 4315

(http://iopscience.iop.org/0953-8984/8/23/021)

J. Phys.: Condens. Matter **8** (1996) 4315–4323. Printed in the UK

Zn, Mn and Te K-edge EXAFS studies of the diluted magnetic semiconductor $Zn_{1-x}Mn_xTe$

N Happo†, H Sato†, T Mihara†, K Mimura†, S Hosokawa†, Y Ueda‡ and M Taniguchi†

† Faculty of Science, Hiroshima University, Kagamiyama 1-3, Higashi-Hiroshima 739, Japan
‡ Tokuyama National College of Technology, Kume-Takajo 3538, Tokuyama 745, Japan

Received 9 August 1995, in final form 25 January 1996

Abstract. Extended x-ray absorption fine-structure measurements at the Zn, Mn and Te K edges of the diluted magnetic semiconductors $Zn_{1-x}Mn_xTe$ ($x \leqslant 0.65$) have been performed to investigate the local coordination around each of the atoms. The nearest-neighbour and next-nearest-neighbour interatomic distances are found to be almost unchanged on changing the Mn concentration (x). These results indicate that the tetrahedral $ZnTe_4$ and $MnTe_4$ clusters are embedded in the alloys with a well-preserved form, in agreement with the x-independent Mn 3d partial density of states derived from resonant photoemission measurements.

1. Introduction

Ternary $Zn_{1-x}Mn_xTe$ alloys belong to a group of materials known as diluted magnetic semiconductors (DMSs), where the cations Zn are randomly replaced by substitutional magnetic Mn^{2+} ions in zinc-blende structure for the Mn composition (x) up to 0.86 [1, 2]. DMSs have attracted considerable attention because of their striking magnetic [3–8] and magneto-optical properties [9–17]. In such phenomena, a hybridization of the Mn 3d states with the sp-band states plays an important role. The degree of the hybridization is strongly affected by the local coordination around the Mn atom.

Resonant photoemission measurements in the Mn 3p–3d excitation region have revealed that the Mn 3d partial density of states (DOS) in $Zn_{0.7}Mn_{0.3}Te$ is very similar to that in $Cd_{0.8}Mn_{0.2}Te$ [18]. From the configuration interaction (CI) theory with the $MnTe_4$ cluster model [19], the similarity of the Mn 3d partial DOS suggests that the bond distances of tetrahedral $MnTe_4$ clusters in $Zn_{0.7}Mn_{0.3}Te$ and $Cd_{0.8}Mn_{0.2}Te$ are almost equal to each other, though x-ray diffraction (XRD) measurements [20] show that the lattice constant of $Zn_{0.7}Mn_{0.3}Te$ is somewhat shorter than that of $Cd_{0.8}Mn_{0.2}Te$.

Recently, we have performed resonant photoemission measurements for $Zn_{1-x}Mn_xTe$ ($0.08 \leqslant x \leqslant 0.65$) and found that the Mn 3d partial DOS remains almost unchanged as x changes [21]. These results suggest that the local coordination around the Mn atoms in $Zn_{1-x}Mn_xTe$ is well preserved over the range of x from 0.08 to 0.65.

In the light of results on the electronic structure of $Zn_{1-x}Mn_xTe$, we have made extended x-ray absorption fine-structure (EXAFS) measurements to investigate the local structure. EXAFS is an ideal structural probe for disordered systems such as random alloys. We report the results for the Zn–Te, Mn–Te and Te–Te interatomic distances, and the bond angles of $ZnTe_4$ and $MnTe_4$ clusters derived from the Zn, Mn and Te K-edge EXAFS

0953-8984/96/234315+09$19.50

spectra. We discuss the relation between the local coordination around the Mn atom and the Mn 3d states.

2. Experimental procedures

$Zn_{1-x}Mn_xTe$ ($x = 0.16$, 0.24, 0.32, 0.47, 0.60 and 0.65) single crystals were grown by the Bridgeman method. We confirmed that the samples formed a homogeneous crystal phase of zinc-blende type by XRD. The x-value was determined by electron-probe microanalysis (EPMA). The well-ground powder of the sample was mixed with BN and pressed into a pellet with a diameter of 10 mm. The Zn K-edge (9660.7 eV) and Mn K-edge (6537.6 eV) EXAFS spectra were measured at BL-7C of the Photon Factory in the National Laboratory for High Energy Physics (KEK-PF). The Te K-edge (31 811.4 eV) spectra were measured at BL-14A of KEK-PF. The storage ring was operated with a ring energy of 2.5 GeV and a ring current of 360–250 mA. Si(111) and Si(553) crystals were used as double-crystal monochromators for measurements of the Zn and Mn, and Te K-edge spectra, respectively. All spectra were measured in the transmission mode. The intensities of the incident and transmitted x-ray beams (I_0 and I) were monitored using two ionization chambers. As the detector gases introduced into the chambers for measuring I_0 and I, we used pure N_2 and N_2(90%)–Ar(10%) for the Zn, He(90%)–N_2(10%) and pure N_2 for the Mn, and pure Kr and pure Kr for the Te K-edge EXAFS measurements, respectively. In the case of the Mn K-edge measurements, higher-harmonic x-rays were minimized by detuning the monochromator to 50% of the fundamental intensity. All of the measurements were performed at 60 K, since it is difficult to obtain information on next-nearest-neighbour distances at 300 K due to the thermal vibration, which reduces the amplitude of the EXAFS oscillations.

Table 1. R-ranges of Fourier filterings and k-ranges of curve fittings of the Zn, Mn and Te K-edge EXAFS analysis.

	Zn K edge	Mn K edge	Te K edge
R-range			
(main peak)	1.9–2.7 Å	2.0–2.8 Å	1.5–2.7 Å
(second peak)			3.4–4.5 Å
k-range	3.0–18.0 $Å^{-1}$	3.0–14.0 $Å^{-1}$	3.0–12.5 $Å^{-1}$

3. Data analysis

The EXAFS function, $\chi(k)$, was obtained by the standard procedure [22]: pre-edge and post-edge background subtraction and subsequent normalization with the atomic absorption coefficients. The values of $\chi(k)$ multiplied by k^2 and the Hanning window function were Fourier transformed into R-space. The magnitude of the Fourier transform, $|F(R)|$, was filtered around the first or second peaks and inverse Fourier transformed into k-space. The resulting Fourier-filtered spectrum, $\chi^*(k)$, was curve fitted with the following conventional EXAFS formula:

$$\chi^*(k) = NB(k)\exp[-2\sigma^2k^2]\sin[2kR + \phi(k)]/kR^2. \quad (1)$$

Here $B(k)$ and $\phi(k)$ are the backscattering amplitude and the total phase shift between the absorber and scatterer, respectively. N, R and σ^2 are the coordination number, interatomic

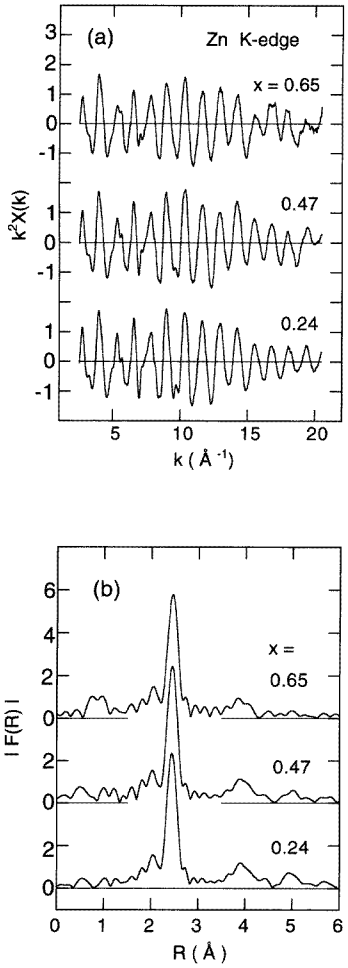

Figure 1. (a) The EXAFS function, $k^2\chi(k)$, and (b) the magnitude of the Fourier transform, $|F(R)|$, for the Zn K-edge data for $Zn_{1-x}Mn_xTe$ ($x = 0.24$, 0.47 and 0.65) measured at 60 K.

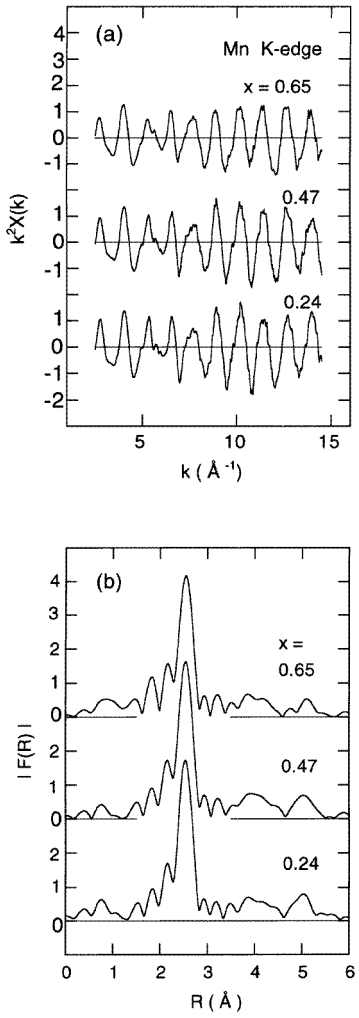

Figure 2. (a) The EXAFS function, $k^2\chi(k)$, and (b) the magnitude of the Fourier transform, $|F(R)|$, for the Mn K-edge data for $Zn_{1-x}Mn_xTe$ ($x = 0.24$, 0.47 and 0.65) measured at 60 K.

distance and mean square relative displacement (MSRD) of each shell atom surrounding the absorber, respectively.

Figures 1(a), 2(a) and 3(a) show $k^2\chi(k)$ for Zn, Mn and Te K-edge EXAFS spectra of $Zn_{1-x}Mn_xTe$ ($x = 0.24$, 0.47 and 0.65), respectively. Figures 1(b), 2(b) and 3(b) show the respective $|F(R)|$ (absolute values only). The main peaks at around 2.4 Å and 2.6 Å of $|F(R)|$ in figure 1(b) and 2(b) are attributed to nearest-neighbour Te atoms around Zn and Mn, respectively. The main peak at around 2.3 Å of $|F(R)|$ in figure 3(b) originates from nearest-neighbour Zn and Mn atoms around Te atoms, and the second peak at around 4 Å is ascribed to next-nearest-neighbour Te atoms. In the data analysis, the R-ranges of the Fourier filterings and the k-ranges of the curve fittings are shown in table 1.

$B(k)$ and $\phi(k)$ were derived from standard materials. We used a zinc-blende-type ZnTe

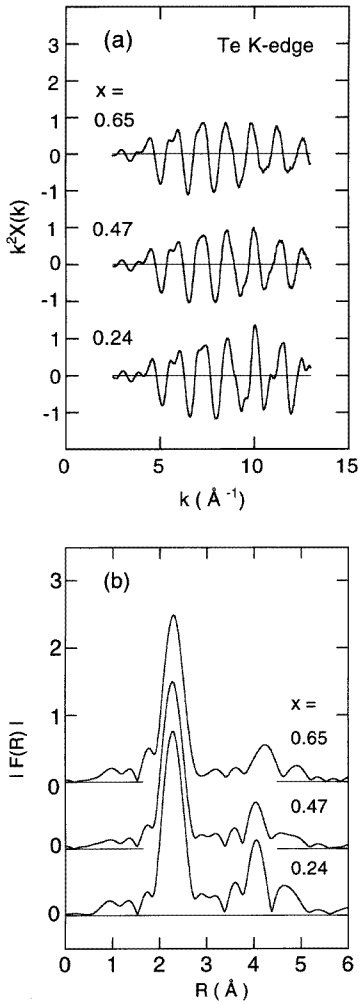

Figure 3. (a) The EXAFS function, $k^2\chi(k)$, and (b) the magnitude of the Fourier transform, $|F(R)|$, for the Te K-edge spectra of $Zn_{1-x}Mn_xTe$ ($x = 0.24$, 0.47 and 0.65) measured at 60 K.

and an NiAs-type MnTe for the nearest-neighbour analysis as standards.

The multiple-scattering (MS) effect has to be considered for deriving the structure beyond the nearest-neighbour analysis. Zabinsky *et al* have reported that the mean curved-wave amplitude of triangular paths of next-nearest neighbours (second shell) in $\chi(k)$ for metallic Cu is nearly equal to that of single-scattering paths from the MS calculation using the FEFF program (version 6) [23]. The calculation was, however, performed over the range $0 \leqslant k \leqslant 20$ Å^{-1}. It is known that the MS effect is very large in the low-k-value region.

On the other hand, Diop and Grisenti have reported that the MS contribution is evaluated to be less than 5% for $k \geqslant 3$ Å^{-1} from the MS calculation using the MSXAS code for ZnSe with the zinc-blende structure. Thus, the conventional method can be used without significant loss of accuracy for the second-shell analysis for $k \geqslant 3$ Å^{-1} [24]. We curve fitted $\chi^*(k)$ over the range $3.0 \leqslant k \leqslant 12.5$ Å^{-1} in case of Te K-edge analysis, as shown in table 1.

$\chi(k)$ with the MS effect is different to equation (1). The MS effect is approximately

incorporated into the $B(k)$ and $\phi(k)$ of the standard, as long as the parameters are derived from the standard with the same structure as the sample, because the MS effect of the sample can be assumed to be almost equal to that of the standard.

It is expected that two kinds of bond, Te–Zn–Te and Te–Mn–Te, exist in the second shell around Te atoms in $Zn_{1-x}Mn_xTe$. In order to obtain the $B(k)$ and $\phi(k)$ in the case where the Mn atom locates between the Te atoms, we have to use a zinc-blende MnTe as the standard. However, the structure of MnTe is generally of NiAs type under the thermal equilibrium. Thus, in the case of second-shell analysis, we used only zinc-blende-type ZnTe [25] as the standard. Here, we assumed that the $B(k)$ and $\phi(k)$ including the MS effect of the hypothetical zinc-blende MnTe are nearly equal to those of ZnTe.

In order to decrease the parameter and to make the curve-fitting analysis accurate, we fixed N-values, which are related to x-values obtained from EPMA measurements [26]. For the first shells of Zn and Mn K edges, N[Zn–Te] and N[Mn–Te] were fixed to be 4, while for the Te K edge, N[Te–Zn] and N[Te–Mn] were fixed to be $4(1-x)$ and $4x$, respectively. Here, N[Zn–Te] indicates the coordination number of nearest-neighbouring Te atoms around Zn. Similarly, N[Te–Zn–Te] and N[Te–Mn–Te] were fixed to be $12(1-x)$ and $12x$, respectively, where N[Te–Zn–Te] is the coordination number of next-nearest-neighbouring Te atoms around Te in the case where the Zn atom locates between the Te atoms.

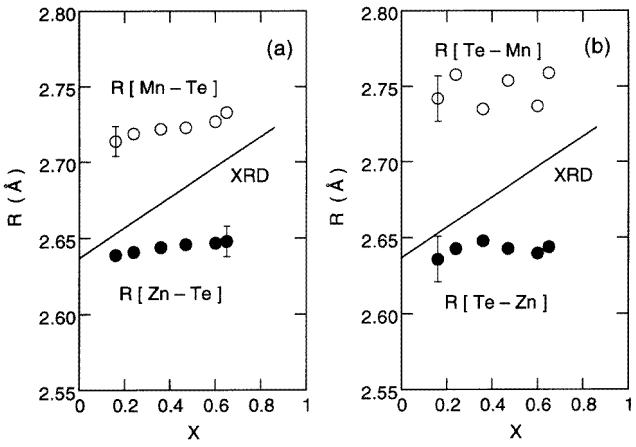

Figure 4. (a) R[Zn–Te] (closed circles) and R[Mn–Te] (open circles) for $Zn_{1-x}Mn_xTe$ as functions of x obtained from the Zn and Mn K-edge EXAFS data. (b) R[Te–Zn] (open circles) and R[Te–Mn] (closed circles) obtained from the Te K-edge EXAFS data. The solid lines show the cation–anion distances obtained from XRD measurements [20] under the VCA.

4. Results and discussion

All of the results for the interatomic distances are shown in table 2. In figure 4(a), the Zn–Te and Mn–Te bond lengths (R[Zn–Te] and R[Mn–Te]) in $Zn_{1-x}Mn_xTe$ as functions of x are indicated by closed and open circles, respectively [27]. The solid lines represent the averaged cation–anion bond lengths derived from XRD measurements [20] under the virtual-crystal approximation (VCA). One notices that R[Zn–Te] and R[Mn–Te] are almost unchanged when x changes, and are nearly equal to the values for pure ZnTe (2.635 Å) and

Table 2. Interatomic distances (in Å) derived from the Zn, Mn and Te K-edge EXAFS analysis. Errors given for the values in the top line apply to all of the values in the column.

x	R[Zn–Te]	R[Mn–Te]	R[Te–Zn]	R[Te–Mn]	R[Te–Zn–Te]	R[Te–Mn–Te]
0.16	2.64 ± 0.01	2.71 ± 0.01	2.64 ± 0.015	2.74 ± 0.015	4.33 ± 0.02	4.49 ± 0.025
0.24	2.64	2.72	2.64	2.76	4.33	4.45
0.36	2.64	2.72	2.64	2.73	4.32	4.44
0.47	2.65	2.72	2.64	2.75	4.34	4.46
0.60	2.65	2.72	2.64	2.74	4.32	4.42
0.65	2.65	2.73	2.64	2.76	4.33	4.46

the hypothetical zinc-blende MnTe (∼2.74 Å), respectively.

We show the results for nearest-neighbour distances from Te K-edge data in figure 4(b). The R[Te–Zn] (open circles) and R[Te–Mn] (closed circles) are consistent with those from the Zn and Mn K-edge spectra. The present results reveal that the VCA is inadequate for $Zn_{1-x}Mn_xTe$. Instead it is Pauling's concept [28] of constant ionic radii that explains the experimental results. Such phenomena have also been reported for the other DMSs, $Cd_{1-x}Mn_xTe$ [29], $Zn_{1-x}Mn_xSe$ [30] and $Hg_{1-x}Mn_xTe$ [31].

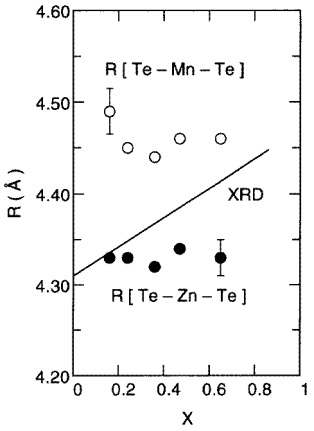

Figure 5. R[Te–Zn–Te] (closed circles) and R[Te–Mn–Te] (open circles) for $Zn_{1-x}Mn_xTe$ as functions of x obtained from the analysis for the second peaks of the Te K-edge $|F(R)|$. The solid line shows the Te–Te distances obtained from XRD measurements [20] under the VCA.

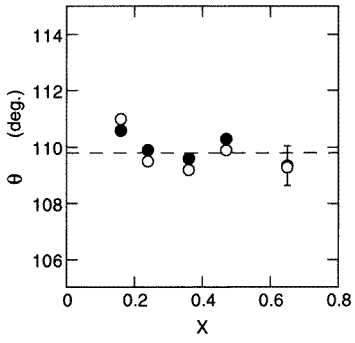

Figure 6. θ[$ZnTe_4$] (closed circles) and θ[$MnTe_4$] (open circles) for $Zn_{1-x}Mn_xTe$ as functions of x calculated from R[Zn–Te] and R[Te–Zn–Te], and R[Mn–Te] and R[Te–Mn–Te], respectively. The dashed line shows the angle of a pure tetrahedron (109.8°).

In contrast to the case for nearest neighbours, there is little information of the next-nearest-neighbour of DMSs except for in the case of $Zn_{1-x}Mn_xSe$ [30]. Te–Te interatomic distances determined from the second peaks of the Te K-edge spectra are shown in figure 5. A solid line shows Te–Te distances obtained from XRD measurements [20]. It should be noticed that there are two kinds of almost x-independent Te–Te distance of about 4.33 and 4.45 Å in $Zn_{1-x}Mn_xTe$. The shorter distance is nearly equal to that of pure ZnTe (4.31 Å), while the other distance is nearly equal to that of the hypothetical zinc-blende MnTe (4.47 Å). Therefore, we assume the short value to be the Te–Te interatomic distance in the case where the Zn atom locates between the Te atoms (R[Te–Zn–Te]). The long

distance, on the other hand, corresponds to R[Te–Mn–Te].

The bond angles of the $ZnTe_4$ and $MnTe_4$ clusters (θ[$ZnTe_4$] and θ[$MnTe_4$]) were calculated from R[Zn–Te] and R[Te–Zn–Te], and R[Mn–Te] and R[Te–Mn–Te], respectively. The results are shown in figure 6. As expected from the derived bond lengths, the bond angles of the clusters are almost independent of x and nearly equal to the value 109.8° of a pure tetrahedron. Thus, we conclude that the $ZnTe_4$ and $MnTe_4$ clusters are embedded in $Zn_{1-x}Mn_xTe$ with a well-preserved form as a result of the strong covalency of the bond between the cation and four-coordinated Te atoms.

The present EXAFS results are in contrast to the VCA results, though the long-range order is still preserved as indicated by XRD [20]. Mikkelsen and Boyce reported that the cation–anion and anion–anion distances of $Ga_{1-x}In_xAs$ derived from EXAFS measurements are almost equal to those in pure GaAs and InAs; however, the cation–cation distances approach those derived from XRD [32]. According to the result, Balzarotti *et al* assumed that the cation sublattice remains undistorted for $Cd_{1-x}Mn_xTe$ as the structural model [29], for which the results of EXAFS are consistent with those of XRD. The second-shell analysis was, however, not performed.

In order to confirm the validity of the Balzarotti's model, the cation–cation distances, R[Zn-Zn], R[Zn-Mn] and R[Mn-Mn], should be analysed. It was, however, difficult to analyse the cation-edge spectra, because of the weak EXAFS oscillations disturbed by the heavy intermediate Te atoms. We have tentatively analysed the second peaks of $|F(R)|$ of cation-edge spectra under the assumption that the cation–cation distances obey the VCA. The curve fitting of the experimental data was, however, not satisfactory.

Wu *et al* have commented on the following in the EXAFS studies on $GaAs_xP_{1-x}$ [33]. The regular tetrahedra obeying the VCA can be obtained by averaging the five tetrahedra, $GaAs_4$, $GaAs_3P$, $GaAs_2P_2$, $GaAsP_3$, GaP_4, though atoms deviate from the ideal lattice positions. Therefore, long-range order is still preserved as in the XRD. EXAFS results are for the average effect over the different coordinations, and XRD reflects the averaged EXAFS results.

Recently, resonant photoemission measurements have revealed the Mn 3d states in the valence bands of $Zn_{1-x}Mn_xTe$ [21]. The Mn 3d partial DOSs exhibit a characteristic feature consisting of three structures: a main peak at 3.75 eV, valence bands at 0–2.5 eV, and a multielectron satellite structure at around 7 eV below the valence band maximum. We have found that the intensities of the valence bands and satellite relative to that of the main peak remain almost unchanged when x is changed. According to a CI theory [19], the spectral shape of the Mn 3d partial DOSs can be reproduced using parameters of $\varepsilon_d - \varepsilon_p + U$ and pdπ, where ε_d and ε_p are energies of unhybridized Mn 3d and Te 5p orbitals, respectively, and U is almost the intra-atomic Coulomb correlation energy of Mn 3d electrons. The value of $\varepsilon_d - \varepsilon_p + U$ is unchanged when x is changed, while the p–d transfer integral, pdπ, strongly depends on features of the local structure, such as the bond length and bond angle of the $MnTe_4$ cluster. We believe that the x-independence originates from the well-preserved form of the tetrahedral $MnTe_4$ cluster.

Finally, we discuss the MSRD. The differences between σ^2 for the Zn–Te bonds in $Zn_{1-x}Mn_xTe$ and that for standard ZnTe ($\Delta\sigma^2$[Zn–Te]) obtained from the Zn K-edge spectra are shown in table 3. The values of $\Delta\sigma^2$[Mn–Te] are also shown in table 3. σ^2 is the sum of a static and thermal component with the following formula:

$$\sigma^2(T) = \sigma_s^2 + \sigma_{th}^2(T) \tag{2}$$

where the subscripts 's' and 'th' indicate the static and thermal parts, respectively [30]. The structural disorder σ_s^2 is essentially independent of temperature, while $\sigma_{th}^2(T)$ arises from the

Table 3. $\Delta\sigma^2$ (in 10^{-4} Å^2) derived from the Zn and Mn K-edge EXAFS analysis. Errors given for the values in the bottom line apply to all of the values in the column.

x	$\Delta\sigma^2$[Zn–Te]	$\Delta\sigma^2$[Mn–Te]
0.16	0.3	−2.2
0.24	2.3	−1.4
0.36	2.4	−1.0
0.47	1.9	−1.1
0.60	2.7	0.3
0.65	5.9 ± 0.5	3.4 ± 0.5

thermal vibration. Since we measured the EXAFS spectra at a fixed temperature, we mainly attribute $\Delta\sigma^2$ to σ_s^2-components. The $\Delta\sigma^2$[Zn–Te] are positive, which means that σ_s^2 for the Zn–Te bonds in $Zn_{1-x}Mn_xTe$ are larger than that in ZnTe, and increase with increasing x. The results indicate that the replacement of Zn with Mn atoms produces distortion in the $Zn_{1-x}Mn_xTe$ lattice and the distortion becomes larger with increasing x. On the other hand, the values of $\Delta\sigma^2$[Mn–Te] are negative for $x \leqslant 0.47$, which suggests that the Mn–Te bond in the alloys is stronger than that of the $MnTe_6$ cluster in the NiAs-type MnTe. The increase of $\Delta\sigma^2$[Mn–Te] with x is in agreement with the tendency of $\Delta\sigma^2$[Zn–Te]. For $x > 0.6$, $\Delta\sigma^2$[Zn–Te] and $\Delta\sigma^2$[Mn–Te] increase remarkably. We believe that the increase of MSRD is related to the limit of the Mn concentration ($x = 0.86$) [1, 2].

5. Conclusion

We have performed EXAFS measurements at the Zn, Mn and Te K edges for $Zn_{1-x}Mn_xTe$ ($0.08 \leqslant x \leqslant 0.65$). The nearest-neighbour interatomic distances, R[Zn–Te] and R[Mn–Te], obtained from the Zn and Mn K-edge EXAFS spectra, are found to remain almost unchanged as x is changed, and to be nearly equal to those of the pure ZnTe and the hypothetical zinc-blende MnTe, respectively. The nearest-neighbour results for the Te K edge support those of the Zn and Mn K-edge analysis.

The next-nearest-neighbour interatomic distances around the Te atom, R[Te–Zn–Te] and R[Te–Mn–Te], are found to be almost constant as functions of x, and to be nearly equal to those of the pure ZnTe and the hypothetical zinc-blende MnTe, respectively.

We conclude that the $ZnTe_4$ and $MnTe_4$ clusters embed in $Zn_{1-x}Mn_xTe$ with a well-preserved form as a result of the strong covalency of the bond between the cation and four-coordinated Te atoms. These results are fully consistent with the x-independent Mn 3d electronic states in $Zn_{1-x}Mn_xTe$ estimated from resonant photoemission measurements in support of the CI theory.

The increases of $\Delta\sigma^2$[Zn–Te] and $\Delta\sigma^2$[Mn–Te] with x suggest that the replacement of Zn with Mn atoms produces a distortion of the $Zn_{1-x}Mn_xTe$ lattice.

Acknowledgments

We are grateful to Professor M Nomura and Professor S Kishimoto, KEK-PF, for technical support for the EXAFS measurements. We thank Mr A Minami, of the Instrument Centre for Chemical Analysis, Hiroshima University, for performing the EPMA measurements. This work was partly supported by a Grant-in-Aid for Scientific Research from the Ministry of Education, Science and Culture, Japan, and Iketani Science and Technology Foundation.

References

[1] Furdyna J K and Kossut J (ed) 1988 *Diluted Magnetic Semiconductors, Semiconductors and Semimetals* vol 25 (New York: Academic)
[2] Jain M (ed) 1991 *Diluted Magnetic Semiconductors* (Singapore: World Scientific)
[3] Diouri J, Lascaray J P and Amrani M E 1985 *Phys. Rev.* B **31** 7995
[4] Peterson D L, Bartholomew D U, Debska U, Ramdas A K and Rodriguez S 1985 *Phys. Rev.* B **32** 323
[5] Bruno A and Lascaray J P 1990 *J. Cryst. Growth* **101** 936
[6] Khattak G D, Keith V and Martin P 1992 *Phys. Status Solidi* a **130** 169
[7] Geibultowicz T M, Fernandez-Baca J A, Nicklow R M, Furdyna J K and Debska U 1993 *J. Appl. Phys.* **73** 5660
[8] Soskic Z, Babic Stojic B and Stojic M 1994 *J. Phys.: Condens. Matter* **6** 1261
[9] Morales Toro J E, Becker W M, Wang B I, Debska U and Richardson J W 1984 *Solid State Commun.* **52** 41
[10] Barilero G, Rigaux C, Menant M, Hau N H and Giriat W 1985 *Phys. Rev.* B **32** 5144
[11] Ves S, Strössner K, Gebhardt W and Cardona M 1986 *Phys. Rev.* B **33** 4077
[12] Lee Y R, Ramdas A K and Aggarval R L 1987 *Proc. 18th Int. Conf. on the Physics of Semiconductors (Stockholm)* ed O Engstrom (Singapore: World Scientific) p 1759
[13] Debowska D, Kisiel A, Rodzik A, Antonangeli F, Zema N, Piacentini M and Giriat W 1989 *Solid State Commun.* **70** 699
[14] Coquillat D, Lascaray J P, Gaj J A, Deportes J and Furdyna J K 1989 *Phys. Rev.* B **39** 10 088
[15] Mertins H-C, Gumlich H-E and Jung C 1993 *Semicond. Sci. Technol.* **8** 1634
[16] Kim Y-G, Kim C-D, Kim H-G, Yang D-I and Kim W-T 1993 *Japan. J. Appl. Phys. Suppl.* 3 **32** 590
[17] Hugonnard-Bruyere S, Buss C, Vouilloz F, Frey R and Flytzanis C 1994 *Phys. Rev.* B **50** 2200
[18] Taniguchi M, Soda K, Souma I and Oka Y 1992 *Phys. Rev.* B **46** 15 789
[19] Mizokawa T and Fujimori A 1993 *Phys. Rev.* B **48** 14 150
Fujimori A and Mizokawa T 1992 *II–VI Semiconductor Compounds* ed M Jain (Singapore: World Scientific) p 103
[20] Yorder-Short D R, Debska U and Furdyna J K 1985 *J. Appl. Phys.* **58** 4056
[21] Happo N, Sato H, Mihara T, Mimura K, Hosokawa S, Taniguchi M and Ueda Y 1994 *Proc. 22nd Int. Conf. on the Physics of Semiconductors (Vancouver)* ed D J Lockwood (Singapore: World Scientific) p 2497
[22] Koningsberger D C and Prins R (ed) 1988 *X-ray Absorption: Principles, Applications and Techniques of EXAFS, SEXAFS and XANES* (New York: Wiley) p 211
[23] Zabinsky S I, Rehr J J, Ankudinov A, Albers R C and Eller M J 1995 *Phys. Rev.* B **52** 2995
[24] Diop D and Grisenti R 1995 *Physica* B **208 + 209** 89
[25] We made the MS calculation for the Te K-edge $\chi(k)$ of ZnTe using FEFF (version 5). The calculation was consistent with the experimental data; therefore, we assume that the $B(k)$ and $\phi(k)$ derived from the standard ZnTe include the MS effect.
[26] We also derived N-values as an adjustable parameter from the EXAFS analysis. The N-values obtained were nearly equal to those derived from EPMA measurements. The uncertainty of the EPMA is, however, less than 1%, and the accuracy is better than that of EXAFS analysis by one order.
[27] Happo N, Sato H, Hosokawa S, Ueda Y and Taniguchi M 1993 *Japan. J. Appl. Phys. Suppl.* 2 **32** 643
[28] Pauling L and Huggins M L 1934 *Z. Kristallogr. Kristallgeom. Kristallphys. Kristallchem.* **87** 205
[29] Balzarotti A, Motta N, Kisiel A, Zimnal-Starmawska M, Czyzyk M T and Podgorny M 1985 *Phys. Rev.* B **31** 7526
[30] Pong W-F, Mayanovic R A, Bunker B A, Furdyna J K and Debska U 1990 *Phys. Rev.* B **41** 8440
[31] Mayanovic R A, Pong W-F and Bunker B A 1990 *Phys. Rev.* B **42** 11 174
[32] Mikkelsen J C and Boyce J B 1983 *Phys. Rev.* B **28** 7130
[33] Wu Z, Lu K, Wang Y, Dong J, Li H, Li C and Fang Z 1993 *Phys. Rev.* B **48** 8694